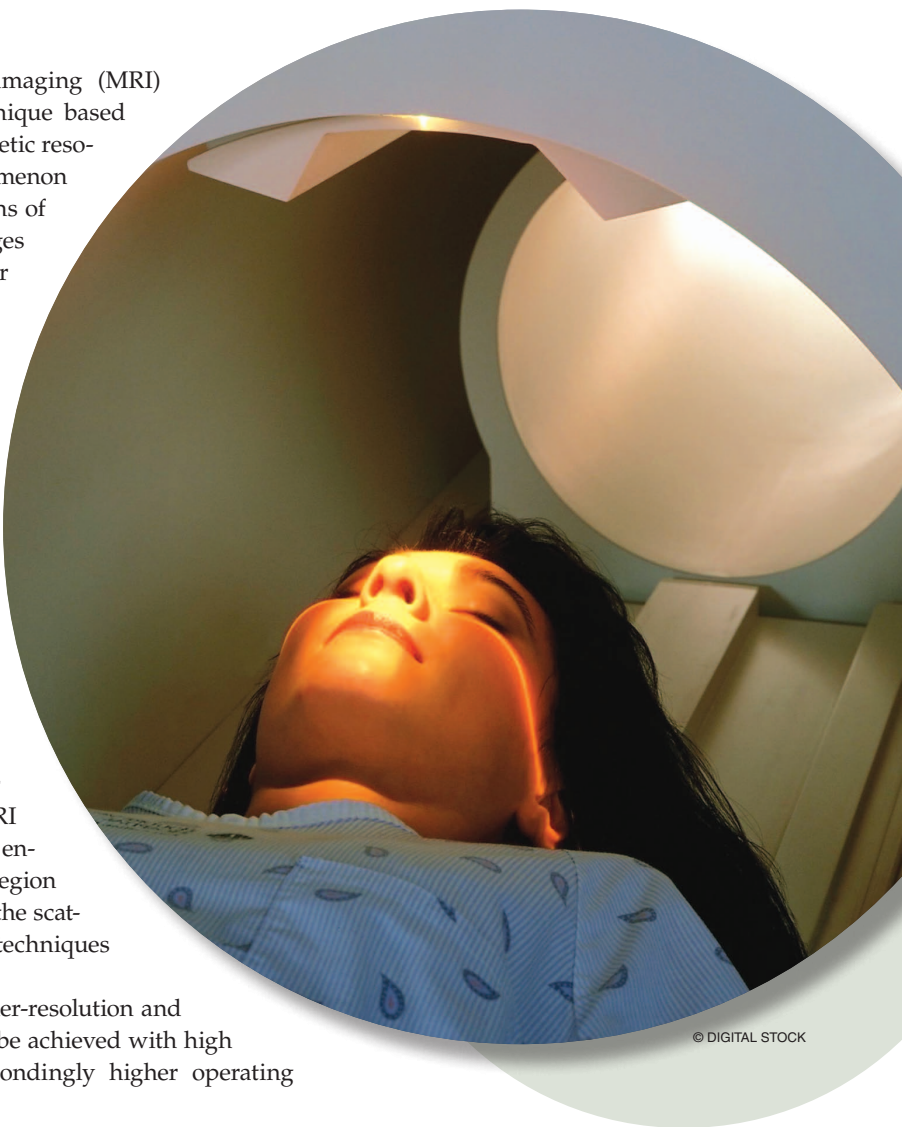


MRI Fundamentals

Robert H. Caverly

Magnetic resonance imaging (MRI) is an imaging technique based on the nuclear magnetic resonance (NMR) phenomenon and provides a means of obtaining detailed, high-contrast images for use by the medical community for diagnostic purposes. MRI differs from other imaging technologies such as single-image X-ray computed tomography scans in that the technique uses nonionizing radiation, relying on static and slowly changing magnetic fields and electromagnetic (EM) energy (primarily in the high-frequency through very-high-frequency bands) to provide soft- and hard-tissue images with outstanding contrast that can be both static and dynamic in nature. High-resolution images of soft tissues from MRI can be obtained even though the wavelength of the EM energy is much larger than the feature size because the MRI process makes use of complex, spatially encoded, reradiated EM signals from the region of interest (ROI) rather than looking at the scattered energy on which other imaging techniques are based.

As medical radiologists ask for higher-resolution and higher-contrast images, these can only be achieved with high magnetic field strengths and correspondingly higher operating



© DIGITAL STOCK

Robert H. Caverly (r.caverly@ieee.org) is with the Department of Electrical and Computer Engineering, Villanova University, Pennsylvania, United States.

Digital Object Identifier 10.1109/MMM.2015.2419753
Date of publication: 5 June 2015

TABLE 1. Widely used MRI species and their AMN and gyromagnetic frequency.

Element	H	C	N	O	F	Na	P	Xe
γ (MHz/T)	42.57	10.7	3.08	5.772	40.08	11.26	17.25	11.7
AMN	1	13	15	17	19	23	31	129

frequencies. The move toward higher operating frequencies should be of interest to those in the IEEE Microwave Theory and Techniques Society (MTT-S) community because many of the theories and techniques developed by us can be used by the MRI community as well. This article covers some of the fundamentals of the MRI process to show the origin of the signals; a knowledge of these fundamentals aids in understanding some of the design tradeoffs that must be addressed by the MRI radio-frequency (RF) engineer. Some details of the past and current MRI technology on both the transmit and receive sides will then be discussed.

MRI Background

MRI is a medical imaging technique based on the NMR phenomenon. Quantum mechanics shows that for a single-proton atomic system (i.e., hydrogen or ^1H), the quantum angular momentum has the same units as the classical angular momentum associated with rotating objects and so is labeled the spin angular momentum, or simply spin. This also occurs with nuclei that contain an odd atomic mass number (AMN), all of which will have a nonzero net spin due to the odd number of protons and/or neutrons. The most commonly studied atomic species in NMR are ^1H and ^{23}Na (sodium 23), but other species are often used for imaging (see Table 1). However, the remaining discussion will assume a single-proton system, ^1H . From a quantum mechanical perspective, quantum mechanical spin gives rise to a magnetic moment associated with the proton. This angular momentum spin \vec{S} is related to the magnetic moment \vec{P} through the gyromagnetic ratio γ ($q/2m$)

$$\vec{P} = \gamma \vec{S}, \quad (1)$$

where q is the electronic charge and m is the mass. In paramagnetic materials, the directions of these spin magnetic moments (or, depending on the audience, you may hear simply spins or magnetic moments) are randomly distributed throughout an object due to thermal energy, yielding a corresponding sum of the individual magnetic moments [net magnetization vector (NMV)] of zero because of this random distribution (Figure 1).

When the object to be imaged is placed in a static magnetic field H (or in terms of magnetic flux, $B_0 = \mu_0 H$); B_0 is usually called the “magnetic field”

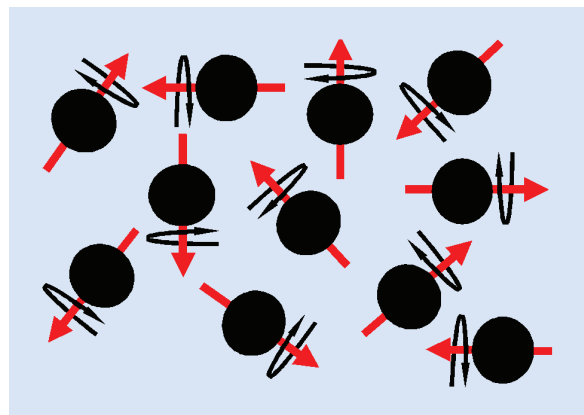


Figure 1. With no external magnetic field applied, the magnetic moments of protons are randomly oriented—i.e., no net magnetization.

in MRI language), torque is experienced by the magnetic moment, leading to a clockwise precession of \vec{P} around the B_0 vector, \vec{B}_0

$$\frac{\partial \vec{P}}{\partial t} = \gamma \vec{P} \times \vec{B}_0. \quad (2)$$

Assuming an $e^{j\omega t}$ variation in \vec{P} , the so-called Larmor frequency can be calculated as $\omega = \gamma B_0$. Table 1 lists the Larmor frequency for some widely used atomic species for MRI; the choice of species is governed by the desired origin of the signal in a certain tissue. The calculations that follow are approximations, and the interested reader is encouraged to see [1] and [2] for more detailed mathematical descriptions.

The applied B_0 field also causes an alignment of the individual magnetic moments, with some of the low-energy spins (n^+) aligned in the same direction as B_0 (so-called spin-up, hence the + sign) and a somewhat smaller number (n^-) exhibiting sufficient energy to align in the opposite direction of B_0 (spin-down) (Figure 2). The difference between the spin-up and spin-down magnetic moments (or energy split of the two quantum states) gives rise to a nonzero NMV, with the magnitude of the NMV governed by the ratio n^-/n^+ obtained using the Boltzmann statistics

$$\frac{n^-}{n^+} \sim \exp\left(-h \gamma \frac{B_0}{kT}\right), \quad (3)$$

where h is the Planck constant, k is the Boltzmann constant, and T is the temperature in Kelvin. For ^1H at 0.25 T, this corresponds to about $10^6 - 2$ spin-down protons per 10^6 spin-up protons; the total number of spins

Magnetic resonance imaging is an imaging technique based on the nuclear magnetic resonance phenomenon.

per unit volume is then approximately $2n^+$ since there are nearly an equal number of spin-up and spin-down protons. The number of proton spins that gives rise to the net magnetic moment per unit volume (V) in the ROI is the difference between the spin-up and spin-down individual proton spins per unit volume, with the NMV related to this proton spin difference

$$|\text{NMV}| \propto (n^+ - n^-) \sim n^+ \left[1 - \exp\left(-h\gamma \frac{B_0}{kT}\right) \right] \sim \left(n^+ h \gamma \frac{B_0}{kT} \right) \quad (4)$$

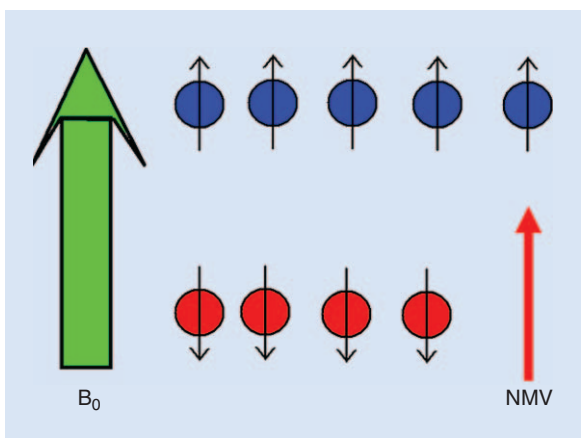


Figure 2. The NMV is related to the difference in magnetization between low-energy spin-up protons n^+ (blue) and higher-energy spin-down n^- (red) magnetic moments.



Figure 3. A high-field MRI scanner with a solenoid high-field coil. The most homogenous region of the B_0 field strength is approximately halfway down the magnet bore. (Photo courtesy of Wikimedia Commons [8].)

with a uniform distribution of spins within the volume assumed. This is an important assumption because it implies that the B_0 field is homogenous within the volume, which in practice ultimately limits the region within the magnet bore that can be used for imaging.

This assumption of field homogeneity requires careful design of the static B_0 magnet to ensure uniformity of one part per million or better over the ROI. An estimate of the number of spins n^+ can be computed based on the fraction of ^1H in water and water density and is approximately 10^{22} spins per cubic centimeter (cc); thus, for $B_0 = 1$ T, there are approximately 10^{17} spins/cc ($n^+ - n^-$) contributing to the NMV. Another feature in (2) is that the NMV is the precessing field picked up by the RF coil open in the transverse plane, and so for a fixed number of spins in a fixed volume in the ROI, increasing B_0 increases the MRI signal. An increase in the so-called spin density in the ROI, such as that which occurs with tissues of different density, and, therefore, different ^1H concentrations, increases the induced EM frequency (EMF) from the NMV as well.

The highest-field MRI magnets are based on superconductor technology and are in the shape of a solenoid (Figure 3) with the most homogeneous region of the magnetic field near the center of the bore. Much research work is being done on optimizing the layout and windings of the superconducting coil to increase the homogeneity within the magnet bore [3]–[7] with EM simulations of field distributions playing an important role.

The application of an RF pulse with sufficient power (with a magnetic flux component called “ B_1 ,” sometimes called the “ B_1 field”) and duration (T_{pulse}) at the Larmor frequency will cause this energy to be absorbed and the magnetic moments to become coherent, with the NMV “flipping” from alignment with B_0 in the longitudinal plane into the transverse plane (the so-called 90° flip angle). The flip angle can be approximated as

$$\Theta_{\text{flip}} \approx 2\pi\gamma \cdot B_1 \cdot T_{\text{pulse}}. \quad (5)$$

For a $B_0 = 1$ T single-proton system with $B_1 = 10 \mu\text{T}$ applied RF, the pulselength to achieve a 90° flip angle ($\Theta_{\text{flip}} = \pi/2$) is approximately $500 \mu\text{s}$. From (5), note that any flip angle is possible depending on the strength of the applied RF field and its duration; for the remaining discussion, 90° flip angles will be assumed. Even though the NMV flips 90° , the NMV is still precessing at the Larmor frequency but now in the transverse plane. A well-positioned RF coil, open to the transverse plane, will have an EMF induced by the NMV through Faraday’s Law of Induction as the NMV sweeps by the plane of the coil (Figure 4). The induced EMF is proportional to the frequency, the applied RF B_1 field, and the NMV (4) as well as the capture area of the RF coil. Note that in (6), the maximum EMF is

achieved if B_1 and the NMV have zero phase angle between them; this implies that B_1 should be circularly polarized

$$\text{EMF} \propto \omega \int \vec{B}_1 \cdot \vec{\text{NMV}}_{xy} dV. \quad (6)$$

There is a problem, however, with picking up the induced EMF in the transverse plane RF coil; the NMV from the ROI volume is very weak since it originates from precessing atomic spins at the Larmor frequency; the applied B_1 field is overwhelmingly strong at the same frequency, which completely masks the desired signal from the ROI. Removal of the B_1 field then allows sensitive RF electronics to pick up the weak NMV-induced EMF. Once the B_1 field is removed, however, the source of energy that flips the NMV into the transverse plane is now removed and the NMV will immediately begin to return to its equilibrium state in the longitudinal plane, aligning with B_0 . This process is referred to as “free induction decay (FID).” The NMV exhibits two time constants in its return to equilibrium through FID that reflect different processes occurring at the atomic level: spin-lattice relaxation (T_1 time constant) and spin-spin relaxation (T_2/T_2^* time constant). The spin-lattice relaxation is the time of return or transfer of energy absorbed by the applied B_1 field (now off) to the surrounding atoms and the return time to B_0 alignment and is strictly a longitudinal plane phenomenon. The spin-spin relaxation is a measure of the loss of a signal due to interaction between neighboring spins and the corresponding loss of coherence (so-called dephasing); the T_2/T_2^* decay describes the loss of a signal in the transverse plane. The T_2^* time constant (called “ T_2 -star”) is generally used since this factor includes effects due to other relaxation mechanisms such as localized magnetic field inhomogeneities (Figure 5).

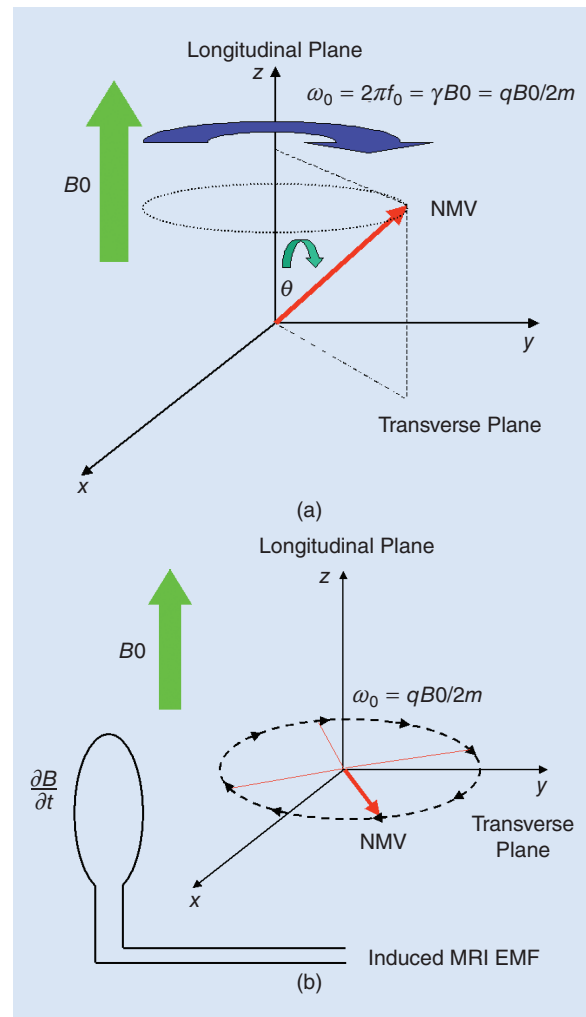


Figure 4. (a) The application of an RF pulse (B_1 field) begins to tip the NMV from the longitudinal plane into the transverse plane. (b) The NMV fully in the transverse plane, an EMF is induced in a coil placed orthogonal to B_0 as the NMV sweeps by the plane of the coil.

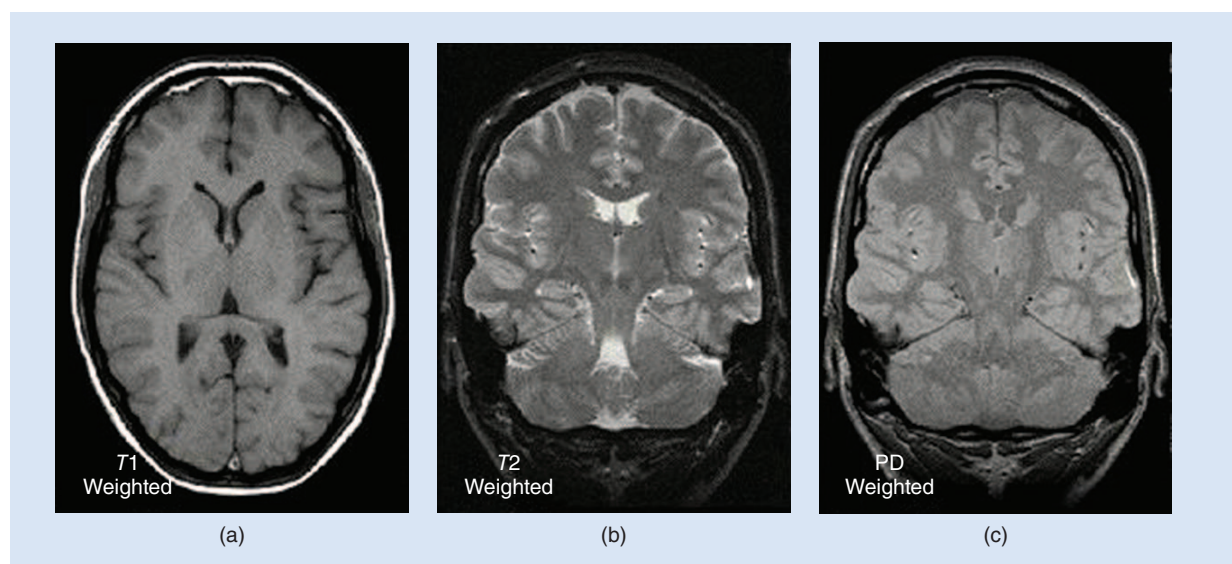


Figure 5. Examples of (a) T1 weighted, (b) T2 weighted, and (c) proton density (PD) weighted MRI scans [9].

The highest-field MRI magnets are based on superconductor technology and are in the shape of a solenoid.

The application of a static B_0 field aligns the magnetic moments of a specimen with B_0 , and the application of a strong B_1 RF field at the Larmor frequency will flip the NMV into the transverse plane so that the MRI signal can be received. In a specimen such as the human body, the NMV in the ROI is precessing at the same frequency throughout the body and so the receive coil system will not be able to discern one location from another, a basic requirement in any imaging system. Work done by some of the pioneers of MRI including Paul C. Lauterbur and Sir Peter Mansfield (winners of the 2003 Nobel Prize in Physiology or Medicine), Raymond Damadian, Robert Gabillard, Herman Carr, and Edwin Purcell showed that spatial localization of the NMR signal could be performed by the use of magnetic field gradients. These gradients add or subtract from the main B_0 field in each of the three Cartesian dimensions $x-y-z$ so that the corresponding Larmor frequencies of the precessing spins and corresponding NMVs also become a function of the position.

If we look at the spatial encoding set up by a magnetic field gradient given by the expression $m_z z$ in only the z -direction (B_0 direction), the Larmor frequency can be written as

$$\omega(z) = \gamma B_0 + \gamma m_z z = \omega_0 + \gamma m_z z. \quad (7)$$

If an RF pulse (B_1) with a rectangular frequency response $2\Delta F$ centered on f_{center} is applied periodically (time between pulses defined as TR, as shown Figure 6), only those spins in the region centered on

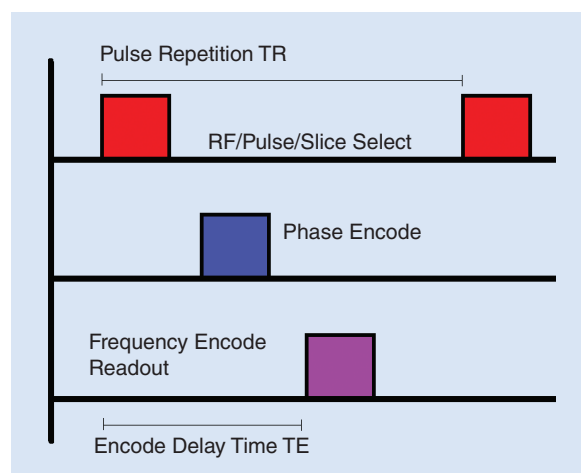


Figure 6. A simplified pulse sequence showing the timing of the slice select, phase encode, and frequency encode/readout signals. The pulse repetition rate TR and echo delay time TE are also shown.

$z_0 = (F_{center} - F_0)/\pi\gamma m_z$ with thickness $\Delta z = \Delta F/\pi\gamma m_z$ will be flipped (Figure 7). This is a very important result from a diagnostic perspective since this excitation process has flipped spins only in a small “slice” of the entire body or specimen and is often called the “slice-select” pulse in the MRI process. Using ^1H as an example, a 5-mT/m z -gradient (m_z) in a 1-T magnetic field for a 5-mm-thick slice requires a pulsed bandwidth of less than 8 kHz. Pulses that are more complex in the frequency domain can be used to excite slices at different locations simultaneously. Once the RF pulse is removed, the flipped NMV begins to return to equilibrium and so the remaining gradients in the x and y directions need to be quickly applied to encode the MRI signal in the remaining two dimensions. These gradients are switched as part of the “phase encoding” and “frequency encoding” process in the MRI pulse sequence (Figure 7). The desired MRI signal is then “read out” during the “frequency encoding” stage of the pulse sequence (TE).

The same concept of magnetic field gradients can be applied to encode signals in the ROI in the remaining two dimensions. The total time-varying phase of the NMV signal in x and y once the z -dimension slice has been selected can be written as

$$\varphi(x, y, t) = \omega_0 t + \gamma m_x x t + \gamma m_y y t, \quad (8)$$

so that the received signal that comes from the NMV and the associated spin density can be approximated as

$$\begin{aligned} S(t) &\propto \int_{\text{ROI}} \omega(\vec{B}_1 \cdot |\text{NMV}(x, y)| e^{-j\varphi(x, y, t)}) dx dy \\ &\propto \int_{\text{ROI}} \omega(\vec{B}_1 \cdot |\text{NMV}(x, y)| e^{-j(\omega_0 t + \gamma m_x x t + \gamma m_y y t)}) dx dy. \end{aligned} \quad (9)$$

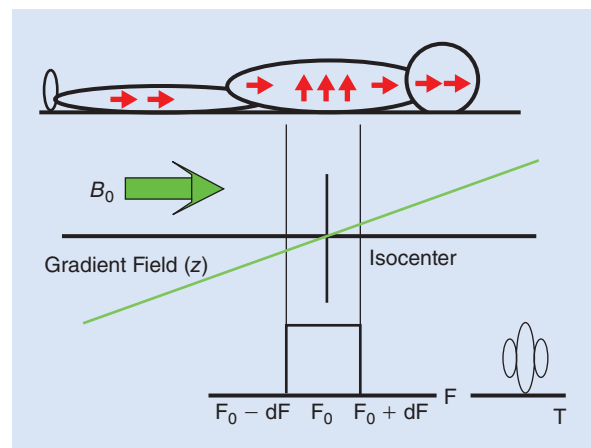


Figure 7. A specific location or “slice” where the NMV is exclusively flipped in the patient can be chosen with appropriate application of a gradient magnetic field in the direction of B_0 and an RF pulse with a rectangular frequency spectrum.

During the phase encode pulse, only an x -directed magnetic field gradient is applied ($m_y = 0$) for a short time T_x ; when the x -directed gradient is turned off, the spins return to the original Larmor frequency but are now out of phase by an amount $\gamma m_x T_x = k_x$ (Figure 8). During the frequency encode pulse, the x -gradient $m_x = 0$, and the Larmor frequency now becomes y -dependent

$$S(t) \propto \int_{\text{ROI}} \omega (\vec{B}_1 \cdot |\text{NMV}(x, y)| e^{-j(\omega_0 t + k_x x + k_y y)}) dk_x dk_y, \quad (10)$$

where $k_y = \gamma m_y t$. This form for $S(t)$ has the appearance of the Fourier integral, and so calculating the inverse Fourier transform of $S(t)$ provides a measure of the $\text{NMV}(x, y)$ that is, in turn, related to the spin density through $\text{NMV}(x, y)$. What is not shown in the expression for $\text{NMV}(x, y)$ but has been assumed all along is that the x - y distribution of spin density is generated by spatially homogenous B_0 and spatially homogenous applied B_1 fields.

Any inhomogeneities in the x - y plane of these magnetic flux components will degrade the $\text{NMV}(x, y)$ from its ideal and result in image degradation. Significant constraints are placed on the RF electronics since the components of $S(t)$ are related to both amplitude (no extraneously produced frequencies) and phase and the electronics must be very linear in these two components. Note that the RF coil is not picking up a signal that directly yields the image but rather the RF coil detects the Fourier representation of the image in so-called k -space. Note in (10) that the x -phase change is dependent on the phase-encode pulse length T_x , whereas the y -phase change is time-dependent. This subtle difference in temporal definitions requires repeating the phase encode step many times to obtain a single image, a total process that can take many minutes in constructing the desired image. In the basic spin-warp imaging process, the phase encode pulse sets up k_y information for a given k_x value, and so a series of measurements of k_x for a line of k_y is performed. If a 256×256 k -space representation is used with a pulse repetition rate of 1 k_x measurement per second, it will take 256 s or

The NMV exhibits two time constants in its return to equilibrium through FID that reflect different processes occurring at the atomic level.

approximately 4 min to obtain a single image. From this point, the digitized RF signal is a form that our colleagues in the signal and image processing communities can take over to generate the image as well as compensate for items that degrade the image such as potential image aliasing, patient movement, and other nonidealities that can be corrected using sophisticated techniques. The remainder of this article will focus on the RF and microwave aspects of the MRI hardware and system requirements. For those interested in the signal and image processing side of the MRI system, *IEEE Signal Processing Magazine* published a special issue in July 2010 with a number of excellent references on this topic [10], [11].

RF Aspects of MRI

Just as in conventional RF and microwave communication systems, the designer and user wish to have the strongest signal available for the lowest transmit power and the lowest noise. In the MRI community, obtaining a high signal-to-noise ratio (SNR) leads to higher resolution and higher-contrast images, providing better images for radiologists and other medical practitioners to perform their diagnostic analysis. From the RF side, the transceiver system for MRI looks remarkably similar to transceivers used in communications and radar applications. The same bottom line in those systems applies in the MRI system as well—maximizing the SNR $S(t)/N$. Among the various RF aspects influencing the SNR in the MRI system are the following:

- the magnitude of the NMV (increases with increasing B_0 , which also increases the Larmor frequency and system frequency)
- the magnitude and homogeneity of the applied B_1 field that flips the spins into the transverse plane so that they can be received (increases not only with applied RF power but also with choice of transmit coil)
- the electric field component of the applied RF electromagnetic field (which should be small to minimize the conductive losses in the specimen that lead to heating during transmit and noise during receive)
- other noise sources such as coil coupling, coil resistive losses, and cabling (which lead to noise generation and pickup) (Figure 9).

RF Coils

An outstanding reference on RF coils for use in MRI can be found in [12]. This classic collection of articles from well-known researchers in the MRI field covers

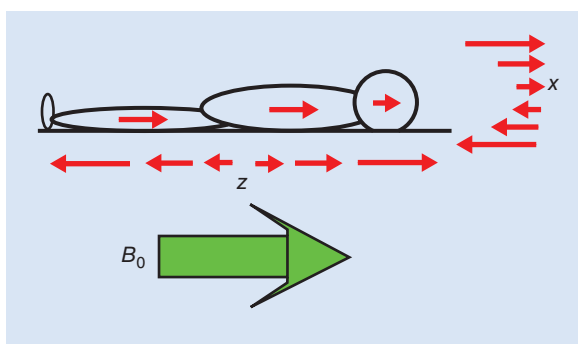


Figure 8. All gradients in the MRI system are in the direction of the main field, B_0 . Only the x - and z -directed field gradients are shown.

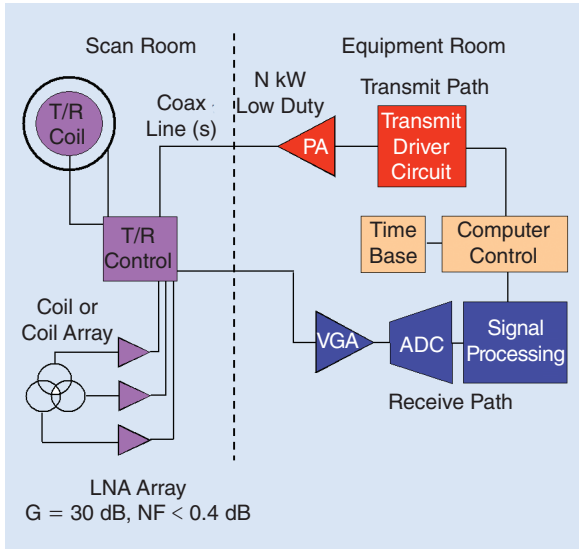


Figure 9. The typical clinical MRI system has the main magnet and low-power electronics in a shielded magnet or scan room, with the main RF power and gradient magnet amplifiers, signal processing, and control systems in a separate equipment room. The low-duty-cycle power N kW can have N kW as high as 30 kW. PA: power amplifier; ADC: analog-to-digital converter; LNA: low-noise amplifier; VGA: variable gain amplifier; T/R: transmit and receive.

surface and volume coils, coil arrays, and electronics. No MRI engineer should be without a copy of this book at his/her desk.

Transmit Coils

In MRI systems, the various coils for transmit and receive are often referred to as "antennas." For B_0 less than about 3 T, the antenna term is a misnomer; at these lower static magnetic fields, the MRI process is primarily a magnetostatic process and not radiative in the EM sense, but is still dependent on the B_1 fields transmitted and the corresponding MRI signal received. Note that in (3), n^+ , the spin density, is directly related to the B_0 field; any inhomogeneity in B_0 will make n^+ a function of position $n^+ \rightarrow n^+(x, y, z)$. Since the amplitude of the received MRI signal originates from n^+ and the xyz -gradients spatially encode the signal, the B_0 -induced inhomogeneity of n^+ over the ROI will degrade the image quality. Since the system is operating magnetostatically, electric fields are small in the specimen, minimizing conductive losses and, hence, patient heating.

The RF excitation is handled by the transmit coil, which is usually physically large in size, with RF energy applied over the entire volume (hence, these transmit coils are sometimes called "volume coils"). The so-called birdcage resonator (or birdcage coil or solenoid) is widely used for MRI systems with a maximum B_0 up to approximately 3 T [12], [13]. The birdcage coil consists of a number of legs or rungs, usually in multiples of four, connected on either side with end rings (Figure 10). The end rings provide a sinusoidal variation in the excita-

These gradients are switched as part of the "phase encoding" and "frequency encoding" process in the MRI pulse sequence.

tion current in the rungs, leading to homogeneous linear magnetic fields in a small region near the interior center of the solenoid. Capacitors placed in the end rings (high pass), legs (low pass), or both (bandpass) are used for tuning; these capacitors need to be able to handle the high pulsed RF power, and the conductors need to be of high conductivity to reduce losses. A 3-dB improvement in SNR due to better coupling between the RF field and the NMV can be obtained by exploiting the degenerate mode in the birdcage coil by providing RF feeds physically 90° apart along the circumference of the coil with a corresponding electrical 90° phase shift (obtained using a quadrature hybrid). Because the birdcage is a resonator, the shorter dimensions of the birdcage coil at a higher B_0 (and, hence, a higher Larmor frequency) are the limiting factor of the birdcage to 3 T and below because a reduction of the end ring diameter means that patients cannot fit inside the solenoid bore; the reduced length to keep the coil at resonance at higher Larmor frequencies also reduces the homogeneous B_0 region. For higher B_0 fields, transverse EM (TEM) resonators are the preferred coil type for a number of reasons, two of the most important being [14]–[22]:

- The bore diameter of the TEM coil is much less dependent on the frequency than the birdcage and can be constructed to fit the magnet bore size.
- Each line element of the TEM resonator can be individually excited, allowing for shaping the RF field pattern to improve the RF excitation homogeneity (so-called B_1 shimming).

The second item is especially important at high B_0 fields because at the associated Larmor frequencies, the system goes from primarily magnetostatic to a system that exhibits EM behavior and full-wave analysis, and design is required. Birdcage coils are still used at very high B_0 fields for small-animal studies since the diameter of the birdcage resonator can be significantly reduced in these applications [23].

The ability to shape/shim the B_1 field using the amplitude and phase control afforded by the TEM transmit coils allows for greater flexibility in improving the image but requires a higher degree of reconfigurability in terms of tuning and matching the individual TEM elements [24]–[26]. A number of papers describing various reconfigurable structures have been published using p-i-n diodes as the switching element, which is required since each TEM element may be excited by a kilowatt or more of RF power [24]–[28].

Transmit coils, whether of the birdcage or TEM type, require retuning and matching due to differences

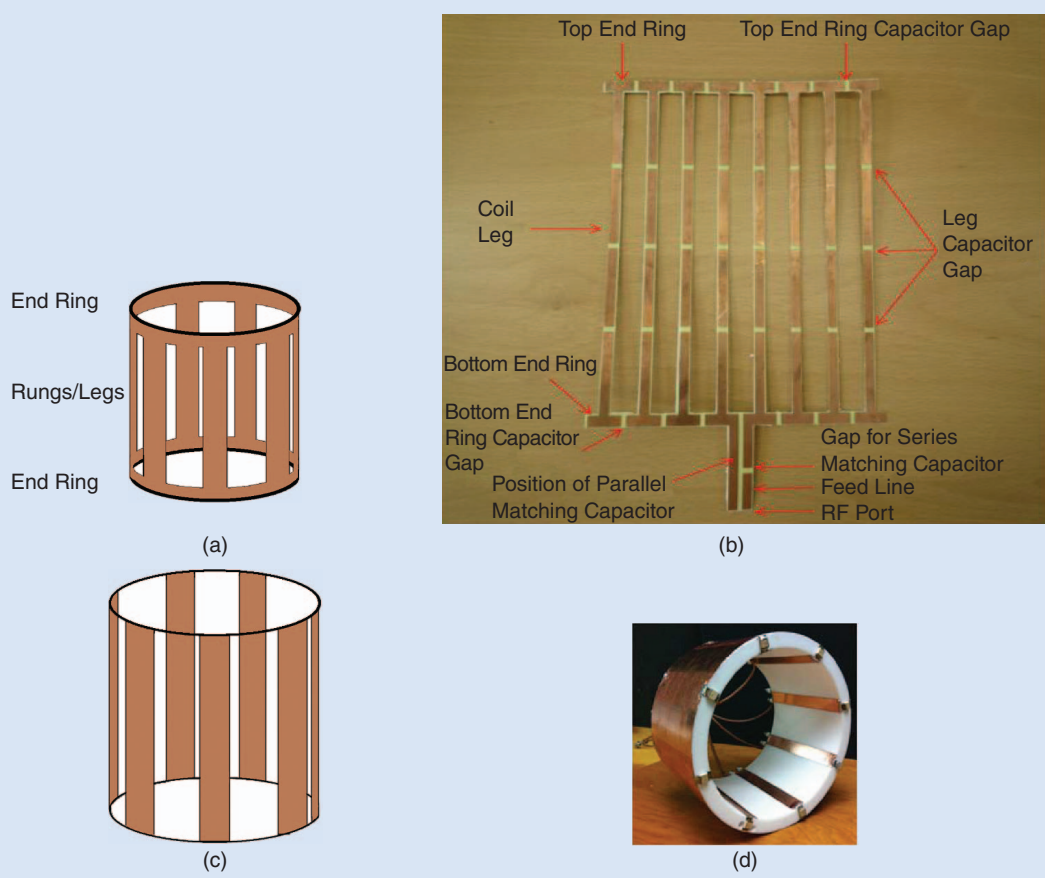


Figure 10. (a) A graphic of a birdcage resonator, (b) an example of a small-animal birdcage resonator (printed layout prior to forming into the cylindrical resonator shape) [62], (c) a TEM resonator graphic, and (d) an example of a TEM resonator [15]. Both resonators provide homogeneous B_1 RF fields in their interiors necessary for uniformly exciting the MRI atomic species.

in dielectric and conductive loading that occur when patients are placed into the MRI system. Automated tuning and matching techniques used in other applications such as automated antenna tuning are often used; these techniques use automated switching of capacitor banks to minimize reflections and retune the coil to the desired Larmor frequency (Figure 11) [24]–[26].

Because of the high-power excitation used in MRI systems, p-i-n diodes are widely used because of their high-power handling and fast switching capability. Modeling

of these devices to ensure low insertion loss and controlled thermal effects is an area of current research [27].

In a similar manner as a single antenna that can be used in any RF or microwave transceiver system, the transmit coil can also be used on receive. The main issue with using the volume coil as a receive coil is that noise originates from the entire volume and is picked up by the coil whereas the signal only originates from a smaller ROI, therefore degrading the SNR of the system. Noise sources include thermal noise from the specimen being scanned as well as resistive losses in the RF coil and cabling. Since the system transmits and receives signals at the same (Larmor) frequency, high-speed, high-power transmit and receive switching is required, another area where p-i-n diodes are used [30]. Receive coils are the subject of a later section.

Higher-field MRI causes a number of issues that were small at lower fields, primarily due to the ROI being a significant fraction of the transmit wavelength. Rather than operating as a magnetostatic system in a low B_0 field environment (around 3 T), the transition to full EM radiation effects starts to occur with standing waves occurring in the patient. These standing waves

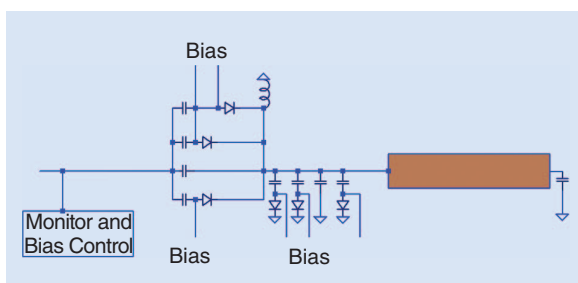


Figure 11. Automated tuning and matching systems using high-voltage capacitors and p-i-n switching diodes are required in all MRI systems.

The designer and user wish to have the strongest signal available for the lowest transmit power and the lowest noise.

do not provide the ideal homogeneous B_1 field that is necessary for uniform spin density excitation; however, with B_1 shimming possible with TEM coils, these effects can be compensated. Much work is being done in the MRI community to improve image quality through RF shimming [31]–[34].

Receive Coils

In early MRI systems, the same birdcage transmit coil was also used for receive (transmit and receive coil). While certainly a useable arrangement, the transmit and receive coil is of large volume (which is why these coils are often referred to as “volume coils”) and so noise pickup due to the integration of the losses over the entire coil volume yielded relatively low SNRs. Many investigators have studied the relationship between signal pickup and noise pickup and for a circular coil of radius r , the signal $S(t)$ and noise $n(t)$ pickup from a pixel point y in the ROI can be described by [35]:

$$S(t) \propto \frac{r^2}{(r^2 + y^2)^{\frac{3}{2}}}; \quad n(t) \propto r^{\frac{3}{2}}; \quad \text{SNR} \propto \frac{r^{\frac{1}{2}}}{(r^2 + y^2)^{\frac{3}{2}}}. \quad (11)$$

The SNR can be maximized at pixel location y_0 if the coil radius is $r_{\text{opt}} = y_0 / \sqrt{5}$. However, as one reduces the size of the coils to maximize the SNR, (11) implies that the field of view becomes quite small, requiring the use of multiple coils (coil array) to perform imaging over a wider area. The multiple-coil array must show minimal coupling between elements to minimize noise sharing; a reduction of the mutual inductance between coils is often achieved by a slight (approximately 20% of the coil radius) overlap of each coil (Figure 12) [36]–[38]. Optimum coil decoupling can be measured on the test bench by driving the two coils with a two-port network

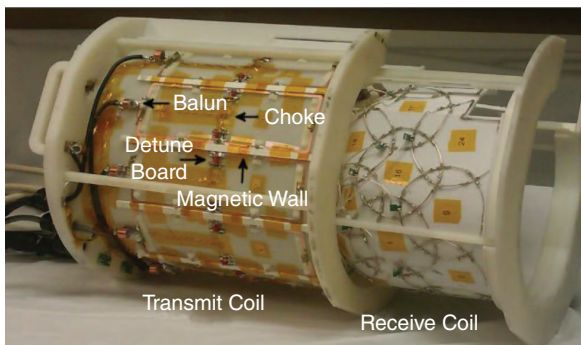


Figure 12. The transmit and receive head coil assembly for use at 7 T [37].

analyzer and observing the minimum S_{21} at specific coil overlaps at the desired Larmor frequency. A single coil (or an array of single coils, often termed a “phased array” [39]) will only pick up the linear component of the circularly polarized NMV. If both components are picked up, a 3-dB SNR improvement will be achieved.

A standard technique for receiving circularly polarized MRI signals is the use of a simple circular coil and a more complex “butterfly” coil to pick up the two circularly polarized components of the field; a 90° hybrid is used to combine the two components into a single signal [35] (Figure 13). The low-noise amplifiers (LNAs) are placed prior to the hybrid to minimize noise.

The use of phased array coils in recent parallel imaging MRI systems provides a reduction in scan time because some of the spatial encoding information previously provided by the magnetic field gradients can be determined from the spatial orientation of the coil array. A variety of schemes used in parallel imaging include sensitivity encoding (SENSE) [40] and simultaneous acquisition of spatial harmonics (SMASH) [41].

Figure 12 shows the receive coil array in very close proximity to both the transmit coil section (outside section of the assembly) as well as the patient (inside the transmit coil assembly). The transmit and receive coil interactions must be minimized since both are tuned to the same Larmor frequency; the use of active and/or passive coil decoupling and detuning schemes are often employed. A simple passive detuning scheme (Figure 14) shows one of the tuning capacitors that tunes the coil to the Larmor frequency. A detuning inductor and antiparallel pair of p-i-n diodes are placed across this tuning capacitor. On receive, the p-i-n diodes are off and the coil is tuned to the Larmor frequency. On transmit, the p-i-n diodes self-rectify using power from the applied RF field, completing the connection of the detuning inductor and rapidly shifting the resonance of the receive coil away from the Larmor frequency. Removal of the RF power causes the p-i-n diodes to turn

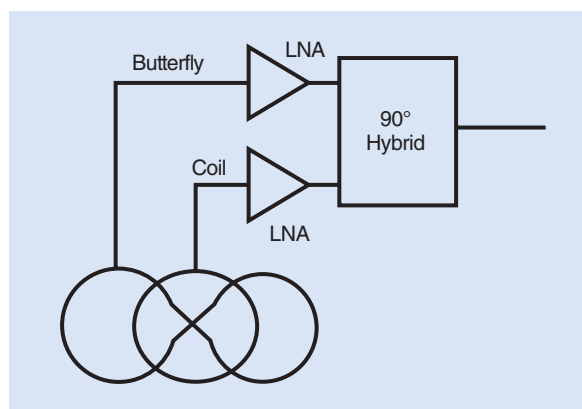


Figure 13. The receiver pickup coils use a simple coil plus an overlapped butterfly coil, LNAs, and a quadrature hybrid to more efficiently pick up the circularly polarized MRI signals.

off with the subsequent shift of the coil resonance back to the Larmor frequency. An active detune circuit using bias inductors and a dc control signal from the system controller can also be used for detuning. In addition to the reduction of coupling with the transmit coil, these coil detuning schemes protect the patient from potential burns during the transmit pulse since the coils are located very close to the patient's skin and provide protection for the sensitive LNAs.

Receivers

Perhaps not surprisingly, the receiver technology for MRI systems is similar to other high-performance receiver systems, with many of the same principles used. For example, LNAs need to be placed close to the signal pickup to keep the overall noise pickup and system noise figure as low as possible. The need to reduce coupling between the receive coils in multicoil arrays adds an interesting design requirement on LNAs. The coupling between coils in the array is dependent on the magnitude of the current flow, and so it is desired to have the coils connected to a high impedance circuit (preamplifier decoupling). Commercial LNAs, however, are typically designed for a $50\text{-}\Omega$ input for both signal and noise matching and so reactive impedance transformation is required between the coil and the LNA [35].

Early MRI systems had long cable runs from the receive coils to LNAs in the equipment room; cable losses and other noise sources yielded images but exhibited poor SNRs. As systems evolved, LNAs were placed in closer proximity to the receive coils in a successful attempt to increase the SNR. In both cases, analog signals were traveling to the equipment room for further signal processing. Down-conversion mixers were used to lower the MRI signal to then-current analog-to-digital converter (ADC) conversion frequencies so that signal processing could be performed in the digital domain (Figure 15). The current trend in MRI receivers is the

The transceiver system for MRI looks remarkably similar to transceivers used in communications and radar applications.

use of multiple parallel channels and direct to digital conversion after the front-end amplifiers, similar to current technology drives to all digital receivers [42], [43]. In an MRI system, digital signals are often sent from the scan room to the equipment room, helping to minimize the noise pickup compared with previously analog-based signal relay techniques. Some research efforts employ the use of optical fibers for the receiver links to the control system [43]. High RF power for flipping the spins must still be generated and relayed via transmission lines to the transmit coils. These techniques mean that a number of electronic subsystems, such as LNAs, gain amplifiers, and ADCs, reside within the bore of the magnet and, therefore, are subject to the large static B_0 field and dynamically changing gradient magnetic fields. While very useful from a signal reception perspective, many commercial electronic components are packaged or constructed with materials such as Kovar (a nickel–cobalt ferrous alloy), which exhibit relatively high magnetic susceptibilities; the resulting residual magnetism in these components can cause unwanted artifacts in the desired MRI image or be susceptible to repeated torquing during gradient switching. The use of low-magnetic-moment device construction and packaging for in-bore use is, therefore, required. Some techniques to reduce the magnetic moment of the packaged components use a combination of paramagnetic and diamagnetic materials to cancel out or lower the overall magnetic susceptibility of the components [44]. Physically moving the electronic components away from the region of high B_0 and B_1 homogeneity in the coil can also be used, but this will involve at least a short transmission line run to the coils with the tradeoff being some loss or noise pickup.

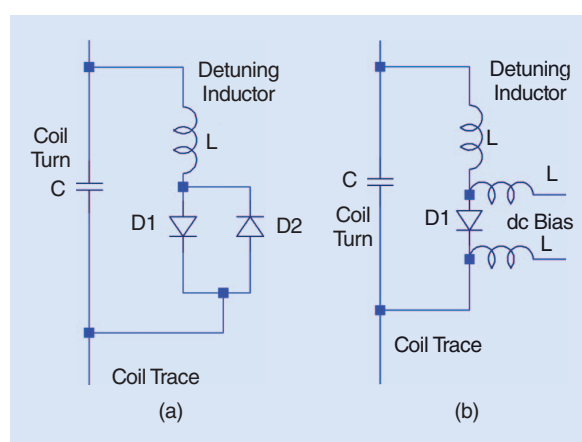


Figure 14. (a) Passive and (b) active p-i-n diode-based circuits for shifting or detuning the resonant frequency of a receiver coil. A redundant detuning and protection system could use both.

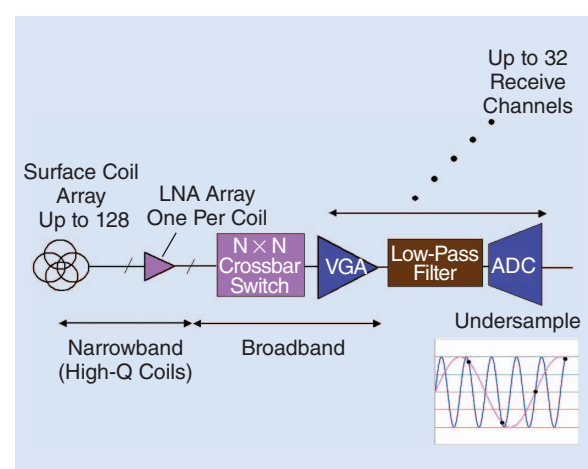


Figure 15. An example of a parallel imaging receiver system.

The multiple-coil array must show minimal coupling between elements to minimize noise sharing.

Transmitters and Power Amplifiers

Transceiver technology for MRI has seen significant improvements along with general electronic technology. On the transmit side, complex waveforms are often required in the various pulse sequences so that specific regions or levels of contrast in the image may be optimized. With the advent of sophisticated signal processing and vector modulators, the waveforms can be created in software and then converted to the required pulse shape (Figure 16). Because of the need to faithfully reproduce these sophisticated waveforms, the power amplifiers (PAs) need to be highly linear and so Class A amplifiers are the rule in MRI work, although there is work on high-power linearized PAs for MRI use. Traditionally, these high-power PAs have been rack mounted and located in a separate room (the so-called equipment room) from the scan room containing the B_0 magnet (Figure 17(a)) [45]. This allowed the heat generated with low-efficiency Class A amplification (and with peak to average power ratio of 6 dB, efficiencies are even lower than the typical Class A PA) to be easily dissipated without heating up the scan room. More recently, PAs have been colocated with the transmit coil within the B_0 magnet bore, eliminating lossy cable runs (Figure 17(b)) [46]. Other researchers are looking at linearization techniques on more efficient but inherently nonlinear amplifiers as a means to reduce excessive PA heating [47], [48]. An abbreviated list of the PA requirements for MRI systems is shown in Table 2. Note the wide frequency range in the table; while the MRI process is relatively narrowband for a specific atomic species being imaged, the wide bandwidth is required so that the same PA can be used in imaging a variety of atomic species with differing gyromagnetic ratios (Table 1).

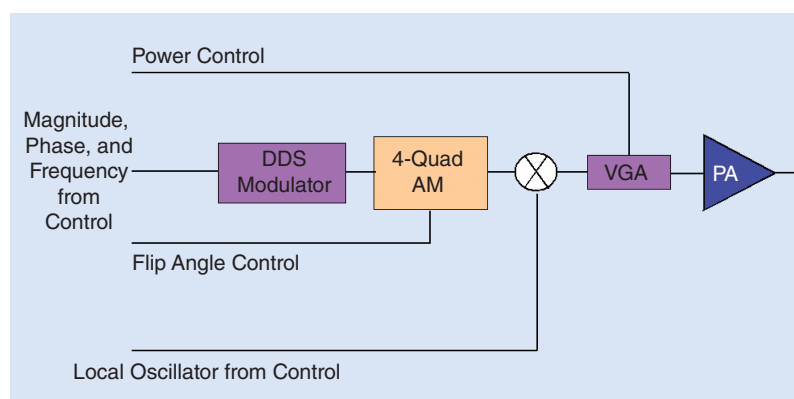


Figure 16. A typical transmitter configuration based on direct digital synthesis (DDS), quadrature amplitude modulation (AM), a variable gain driver (VGA), and final PA.

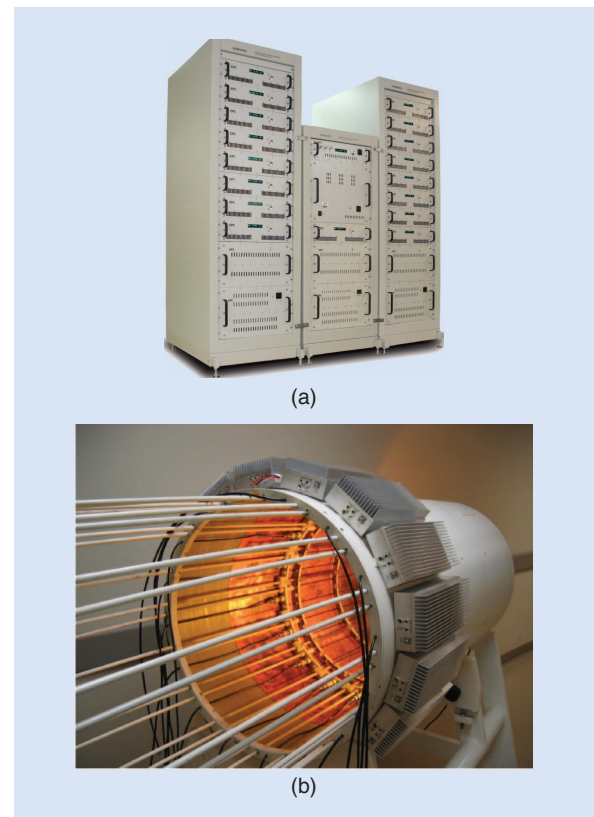


Figure 17. (a) Rack-mounted, 16-channel, 1 kW/channel PAs for a 7-T MRI system [45]. (b) An in-bore PA array with 16 channels, 1 kW/channel [46].

RF Cabling

In many RF applications, not much thought is given to the cable layout other than that based on location constraints, but in the high-power realm of MRI systems, cabling must be carefully considered since cable runs from the equipment to the scan room and/or back can constitute a significant (or even multiple) portion of the operating wavelength. Because of these long lengths, the outer portion of the outer conductor can pick up and conduct significant RF energy (shield currents) along the length of the line, relaying large signals that can create noise or even potentially significant heating. In traditional RF systems, wrapping a number of turns of coaxial line through a ferrite toroid core or slipping the cable through one or more ferrite beads or ferrite clips can perform RF choking of these shield currents.

However, ferrites are one material that should never be used in the proximity of an MRI system, so other techniques need to be employed to reduce these shield currents. One technique involves using a so-called bazooka balun that uses one or more

TABLE 2. PA requirements (9.4 T).

Frequency	30–405 MHz
Bandwidth	1 MHz
Power	Pulse—8 kW CW—100 W
Pulsewidth	20–100 ms (300 ms max)
Duty cycle	10% max
Amplitude rise/fall	500 ns, typical
Output amplitude:	Within 5% to 20 ms
Gain (0 dBm input)	69 dB
Gain flatness	±3 dB
Phase change	<12°
Harmonics	20/12 dBc (second/third)

quarter-wavelength wires, which are open circuited at each end, to provide an RF short. Another technique involves wrapping several turns of coaxial line around a form to create an inductance on the outer side of the outer conductor; the shield insulation is then opened at both ends of this “coil” and a tuning capacitor is inserted, creating a parallel resonant circuit along the outer portion of the shield. This capacitor is then tuned to the Larmor frequency, creating an open circuit to RF shield currents.

Specific Absorption Rate and Other Safety Issues

The typical MRI system uses single or multiple PAs, depending on the system configuration. While these PAs operate in pulsed mode with low duty cycles, they do provide a significant dose of RF energy to the subject being scanned and can raise the tissue temperature in the scanned area. For safety reasons, the RF dose is continuously monitored to ensure that it does not exceed the accepted values; the metric commonly used is the specific absorption rate (SAR), which is defined as the RF power per object mass (weight/kilogram) over a specific exposure time [49] and can be calculated as a partial-body SAR using the International Electrotechnical Commission (IEC) scale for the normal operating mode as [49]

$$\text{SAR} = 10 - 8 \left(\frac{\text{exposed body mass}}{\text{total body mass}} \right) \text{W/kg.} \quad (12)$$

A somewhat less restrictive first-level controlled operating mode SAR can be computed as [49]

$$\text{SAR} = 10 - 6 \left(\frac{\text{exposed body mass}}{\text{total body mass}} \right) \text{W/kg.} \quad (13)$$

A variety of schemes used in parallel imaging include SENSE and SMASH.

Assuming equal exposure to total body mass ratios, (12) and (13) yield SAR values of 2 and 4 W/kg, respectively. Higher SAR values for areas such as the head, trunk, and extremities are in the range of (10–20 W/kg) [49]. These limits vary in different countries but are in general agreement with the IEC limits.

One of the problems with using the SAR as the RF exposure metric for temperature is that the SAR is an averaged value based on the RF power absorption, patient mass, and exposure time. Field inhomogeneities in the scanned subject do occur, especially as one goes to higher B_0 fields and Larmor frequencies, with the result being localized hot spots where the tissue temperature can be significantly higher than the surrounding area [50]. This is especially important if the patient has implants such as pacemakers or stents [49]. Work is currently being done [51]–[56] to study ways to determine and measure the temperature in these hot spots. For example, temperature mapping can be performed by looking closely at phase shifts in the T_1 relaxation time within the ROI [57].

The high static B_0 field can cause magnetic objects to be pulled to it at high speeds (the so-called missile situation) from many meters distance, with the potential for grave injury to those in the magnet's vicinity, patients and health-care professionals alike. Damage to equipment near the scan room, including the magnet itself, has also occurred. Strict protocols regarding materials allowed in the vicinity of the magnet, including implants in the patient (which can cause malfunction, movement, or localized hot spots), must be followed.

The Future

There are a number of areas in the RF portion of the MRI system that are continually under investigation. There is a drive toward large arrays of receive coils (up to 128) in parallel imaging systems to provide good area coverage of the patient as well as reduce the scan time. Reduced scan times down to the tens of millisecond range provide the ability to observe physical processes such as brain function or vascular flow [58] or to assist surgeons during surgery (e.g., interventional MRI [59]). These large parallel receive systems require large numbers of LNAs and ADCs to be within the bore of the magnet; a reduction in the number of these circuits can be performed with various switching matrix techniques. In these cases, physical and size constraints occur and any technique to reduce the footprint will advance the technology.

The drive toward higher B_0 fields for improved resolution and higher tissue contrast (down to

The receiver technology for MRI systems is similar to other high-performance receiver systems.

submillimeter dimensions [60]) is driving advances in high PAs to be able to not only supply the power, switching speed, and bandwidth required for a range of MR species but to also locate the amplifiers in the scan room and magnet bore to reduce losses. In fact, with these higher RF powers and B_1 shimming, new areas of MRI have opened up, including the ability to display conductivity and permittivity information (electrical property tomography) [60]. MRI systems are physically quite large, and a number of investigations are being undertaken to reduce the size to so-called “suitcase” MRI systems. Here, a physically rotatable magnet’s field distribution is used for image encoding instead of gradient coils, reducing the weight and acoustic noise of the scanner, all from a standard power outlet [61].

Not mentioned in this article but certainly an important part of current and future MRI system and component development efforts is, and will continue to be, the extensive use of computer-aided design tools for verifying operation prior to fabrication, for a better understanding of the underlying physics, and for prediction of the SAR and patient heating. Advances in techniques such as the finite-difference time-domain, method of moments and finite-element method analysis, and the associated computing hardware will be better able to predict, and in shorter timeframes, propagation effects and losses in the MRI system; they will also aid in the prediction and design of optimum magnetic field (both B_0 and B_1) configurations for the best SNR and minimized heating. These tools are especially important when high-field MRI is used since B_1 field inhomogeneities due to short wavelengths (compared with the patient) are large and the fields are more radiative in nature rather than magnetostatic as is the case at lower fields.

In addition to the wealth of information available through IEEE Societies such as the MTT-S and the Engineering in Medicine and Biology Society, other avenues of information can be obtained from the *Journal of Magnetic Resonance Imaging* and the *Proceedings of the International Society for Magnetic Resonance in Medicine* (<http://www.ismrm.org>).

References

- [1] A. Omar, *Electromagnetic Scattering and Material Characterization*. Norwood, MA: Artech House, 2011.
- [2] A. Omar, R. Caverly, W. Doherty, R. Watkins, A. Gopinath, and J. T. Vaughan, “A microwave engineer’s view of MRI,” *IEEE Microwave Mag.*, vol. 12, no. 3, pp. 78–86, May 2011.
- [3] M. W. Garrett, “Thick cylindrical coil systems for strong magnetic fields with field or gradient homogeneities of the 6th to 20th order,” *J. Appl. Phys.*, vol. 38, no. 6, pp. 2563–2586, 1967.
- [4] H. Xu, S. M. Conolly, G. C. Scott, and A. Macovski, “Homogeneous magnet design using linear programming,” *IEEE Trans. Magn.*, vol. 36, no. 2, pp. 476–483, 2000.
- [5] S. Chen, Y. Dai, B. Zhao, Y. Li, H. Wang, and K. Chang, “Development of an 8-T conduction—Cooled superconducting magnet with 300-mm warm bore for material processing application,” *IEEE Trans. Appl. Supercond.*, vol. 24, no. 2, pp. 72–76, Apr. 2014.
- [6] C. Wu, J. Guo, C. Chen, G. Yan, and C. Li, “Optimal design and test of main magnet in superconducting MRI,” *IEEE Trans. Appl. Supercond.*, vol. 20, no. 3, pp. 1810–1813, June 2010.
- [7] A. Sattarov, P. McIntyre, and L. Motowidlo, “High field open MRI for breast cancer screening,” *IEEE Trans. Appl. Supercond.*, vol. 25, no. 3, pp. 1–5, June 2015.
- [8] Wikimedia Commons. MRI-Philips.JPG. [Online]. Available: <http://en.wikipedia.org/wiki/File:MRI-Philips.JPG>
- [9] Kieran Maher. (2006). Examples of T1 weighted, T2 weighted and PD weighted MRI scans. [Online]. Available: <http://en.wikipedia.org/wiki/File:T1t2PD.jpg>
- [10] L. Ying and Z. Liang, “Parallel MRI using phased array coils,” *IEEE Signal Processing Mag.*, vol. 27, no. 4, pp. 90–98, July 2010.
- [11] J. A. Fessler, “Model-based image reconstruction for MRI,” *IEEE Signal Processing Mag.*, vol. 27, no. 4, pp. 81–89, July 2010.
- [12] J. T. Vaughan and J. R. Griffiths, Eds., *RF Coils for MRI*, Chichester, U.K.: Wiley, 2012.
- [13] J. Tropp, “The theory of the bird-cage resonator,” *J. Magn. Reson.*, vol. 82, no. 1, pp. 51–62, 1989.
- [14] I. R. O. Connell, K. M. Gilbert, M. A. Abou-Khousa, and R. S. Menon, “Design of a parallel transmit head coil at 7T with magnetic wall distributed filters,” *IEEE Trans. Med. Imaging*, vol. 34, no. 4, pp. 836–845, Apr. 2015.
- [15] S.-M. Sohn, L. DelaBarre, A. Gopinath, and J. T. Vaughan, “Design of an electrically automated RF transceiver head coil in MRI,” *IEEE Trans. Biomed. Circuits Syst.*, vol. PP, no. 99, p. 1, 2014.
- [16] I. A. Elabyad and A. Omar, “An investigation of alternating impedance microstrip transceiver coil arrays for MRI at 7T,” in *IEEE MTT-S Int. Microwave Symp. Dig.*, 2011, pp. 1–4.
- [17] B. Wu, C. Wang, D. A. C. Kelley, D. Xu, D. B. Vigneron, S. J. Nelson, and X. Zhang, “Shielded microstrip array for 7T human MR imaging,” *IEEE Trans. Med. Imaging*, vol. 29, no. 1, pp. 179–184, 2010.
- [18] S. Sung-Min, L. DelaBarre, A. Gopinath, and J. T. Vaughan, “RF head coil design with improved RF magnetic near-fields uniformity for magnetic resonance imaging (MRI) systems,” *IEEE Trans. Microwave Theory Tech.*, vol. 62, no. 8, pp. 1784–1789, 2014.
- [19] M. J. Freire, M. A. Lopez, F. Meise, J. M. Algarin, P. M. Jakob, M. Bock, and R. Marques, “A broadside-split-ring resonator-based coil for MRI at 7 T,” *IEEE Trans. Med. Imaging*, vol. 32, no. 6, pp. 1081–1084, 2013.
- [20] T. Niendorf, “Multi-channel transmit/receive RF coil arrays for cardiac MRI at ultrahigh fields: Design, validation and clinical application,” in *Proc. IEEE MTT-S Int. Microwave Workshop Series RF Wireless Technologies Biomedical Healthcare Applications*, 2013, pp. 1–3.
- [21] I. A. Elabyad, T. Herrmann, J. Bernarding, and A. Omar, “Combination of travelling wave approach and microstrip transceiver coil arrays for MRI at 7T,” in *IEEE MTT-S Int. Microwave Symp. Dig.*, 2011, pp. 1–4.
- [22] C. E. Akgun, L. DelaBarre, Y. Hyoungsuk, S. Sung-Min, C. J. Snyder, G. Adriany, K. Ugurbil, A. Gopinath, and J. T. Vaughan, “Stepped impedance resonators for high-field magnetic resonance imaging,” *IEEE Trans. Biomed. Eng.*, vol. 61, no. 2, pp. 327–333, Feb. 2014.
- [23] T. Cheng, A. W. Magill, A. Comment, R. Gruetter, and L. Hongxia, “Ultra-high field birdcage coils: A comparison study at 14.1T,” in *Proc. 36th Annu. Int. Conf. IEEE Engineering Medicine Biology Society*, Aug. 26–30, 2014, pp. 2360–2363.
- [24] S. Sung-Min, L. DelaBarre, J. T. Vaughan, and A. Gopinath, “ Π (Pi)-matching technique for RF coil of MRI systems,” in *IEEE MTT-S Int. Microwave Symp. Dig.*, 2012, pp. 1–3.
- [25] S. Sung-Min, J. T. Vaughan, and A. Gopinath, “Auto-tuning of the RF transmission line coil for high-fields magnetic resonance imaging (MRI) systems,” in *IEEE MTT-S Int. Microwave Symp. Dig.*, 2011, pp. 1–4.

- [26] S. Sung-Min, L. DelaBarre, J. T. Vaughan, and A. Gopinath, "8-channel RF head coil of MRI with automatic tuning and matching," in *IEEE MTT-S Int. Microwave Symp. Dig.*, 2013, pp. 1–3.
- [27] R. Caverly, W. Doherty, and R. D. Watkins, "Modeling high speed MRI coil switching using PIN diodes," in *IEEE MTT-S Int. Microwave Symp. Dig.*, 2011, pp. 1–4.
- [28] R. Caverly, "Microwave and RF p-i-n diode model for time domain simulation," *IEEE Trans. Microwave Theory Tech.*, vol. 60, no. 7, pp. 2158–2164, 2012.
- [29] R. Caverly, R. Watkins, and W. E. Doherty Jr., "Modeling PIN diode temperature rise in high induced current MR receive coils," in *Proc. Int. Society Magnetic Resonance Medicine*, 2014, vol. 22, p. 1290.
- [30] D. O. Brunner, M. Weiger, T. Schmid, and K. P. Pruessmann, "High-power T/R switches with 350 ns rise time for zero echo time imaging," in *Proc. Int. Society Magnetic Resonance Medicine*, 2014, vol. 22, p. 0922.
- [31] E. A. Attardo, G. Vecchi, and T. Isernia, "Magnetic field shimming in MRI with controlled polarization and SAR limitation," in *Proc. IEEE Antennas Propagation Society Int. Symp.*, July 11–17, 2010, pp. 1–4.
- [32] H. Yi-Cheng, Y. Chu, I.-L. Chern, R. Lattanzi, H. Teng-Yi, and L. Fa-Hsuan, "Mitigate B_1^+ inhomogeneity by nonlinear gradients and RF shimming," in *Proc. Annu. Int. Conf. IEEE Engineering Medicine Biology Society*, 2013, pp. 1085–1088.
- [33] S. X. Xin, H. Qihua, G. Yong, L. Baige, X. Yikai, and C. Wufan, "Fetus MRI at 7 T: B_1 shimming strategy and SAR safety implications," *IEEE Trans. Microwave Theory Tech.*, vol. 61, no. 5, pp. 2146–2152, 2013.
- [34] S. Sung-Min, L. DelaBarre, J. T. Vaughan, and A. Gopinath, "RF multi-channel head coil design with improved B_1^+ fields uniformity for high field MRI systems," in *IEEE MTT-S Int. Microwave Symp. Dig.*, 2012, pp. 1–3.
- [35] A. Reykowski, "Receive arrays," in *Proc. Int. Society Magnetic Resonance Medicine RF Engineering Workshop*, 2009, pp. 1–7.
- [36] P. Angelidis, K. Vassiliadis, and G. D. Sergiadis, "Lowest mutual coupling between closely spaced loop antennas," *IEEE Trans. Antennas Propagat.*, vol. 39, no. 7, pp. 949–953, 1991.
- [37] I. R. O. Connell, K. M. Gilbert, M. A. Abou-Khoussa, and R. S. Menon, "Design of a parallel transmit head coil at 7T with magnetic wall distributed filters," *IEEE Trans Med. Imaging*, vol. 34, no. 4, pp. 836–845, Apr. 2015.
- [38] D. T. P. Nilsson, J. J. Mohr, and V. Zhurbenko, "Practical aspects of ^{13}C surface receive coils with active decoupling and tuning circuit," in *Proc. 42nd European Microwave Conf.*, 2012, pp. 65–68.
- [39] P. B. Roemer, W. A. Edelstein, C. E. Hayes, S. P. Souza, and O. M. Mueller, "The NMR phased array," *Magn. Reson. Med.*, vol. 16, no. 2, pp. 192–225, 1990.
- [40] K. P. Pruessmann, M. Weiger, M. B. Scheidegger, and P. Boesiger, "SENSE: Sensitivity encoding for fast MRI," *Magn. Reson. Med.*, vol. 42, no. 5, pp. 952–962, 1999.
- [41] D. K. Sodickson, "Manning WJ: Simultaneous acquisition of spatial harmonics (SMASH): Fast imaging with radiofrequency coil arrays," *Magn. Reson. Med.*, vol. 38, no. 4, pp. 591–603, 1997.
- [42] C.-L. Lim, P. Serano, and J. L. Ackerman, "Pre-amplifiers for a 15-Tesla magnetic resonance imager," in *Proc. IEEE Int. RF Microwave Conf.*, 2013, pp. 295–299.
- [43] R. Jonas, J. Marjanovic, D. O. Brunner, T. Schmid, U. Moser, B. E. Dietrich, C. Barnet, and K. P. Pruessmann, "In-bore broadband array receivers with optical transmission," in *Proc. Int. Society Magnetic Resonance Medicine*, 2014, vol. 22, p. 0619.
- [44] R. Goldfarb, P. Voskoboynik, W. E. Doherty, Jr., and R. D. Joos, "Low magnetic moment PIN diodes for high field MRI surface coils," *Med. Phys.*, vol. 33, no. 12, pp. 4499–4501, 2006.
- [45] R. Caverly, G. Breed, W. Cantrell, M. Eron, J. Garcia, N. Kondrath, D. Myer, M. Ruiz, and J. Walker, "Advancements at the lower end: Advances in HF, VHF, and UHF systems and technology," *IEEE Microwave Mag.*, vol. 16, no. 1, pp. 28–49, Feb. 2015.
- [46] J. T. Vaughan, L. DelaBarre, T. Jinfeng, S. Sungmin, D. Shrivastava, G. Adriany, and K. Ugurbil, "RF technology for human MRI at 10.5T," in *Proc. IEEE MTT-S Int. Microwave Workshop Series RF Wireless Technologies Biomedical Healthcare Applications (IMWS-BIO)*, 2013, pp. 1–3.
- [47] K. Solbach, A. Abuelhaija, and S. Shooshtary, "Near-magnet power amplifier with built-in coil current sensing," in *Proc. Int. Society Magnetic Resonance Medicine*, 2014, vol. 22, p. 1287.
- [48] J. Y. Lu, P. P. Stang, J. M. Pauly, M. G. Zanchi, and G. C. Scott, "Analysis of gain and noise relationship in RF feedback power amplifier linearization for use at 1.5T MRI," in *Proc. Int. Society Magnetic Resonance Medicine*, 2014, vol. 22, p. 1334.
- [49] Z. Wang and J. C. Lin, "Partial-body SAR calculations in magnetic-resonance image (MRI) scanning systems [Telecommunications Health and Safety]," *IEEE Antennas Propagat. Mag.*, vol. 54, no. 2, pp. 230–237, Apr. 2012.
- [50] Z. Wang and J. C. Lin, "SAR calculations in MRI scanning systems [Health Effects]," *IEEE Microwave Mag.*, vol. 13, no. 5, pp. 22–29, 2012.
- [51] C. Armenean, E. Perrin, M. Armenean, O. Beuf, F. Pilleul, and H. Saint-Jalmes, "RF induced temperature elevation near metallic wires in clinical magnetic resonance imaging," *Magn. Reson. Med.*, vol. 52, pp. 1200–1206, Nov. 2004.
- [52] S. Oh, C. A. Roopnariane, M.-R. Tofighi, and C. M. Collins, "MRI-based temperature and SAR mapping with a new dual-coil solenoid/birdcage heating/measurement system," in *Proc. IEEE Radio Wireless Symp.*, 2010, pp. 520–522.
- [53] C. M. Collins, W. Liu, J. Wang, R. Gruetter, J. T. Vaughan, K. Ugurbil, and M. B. Smith, "Temperature and SAR calculations for a human head within volume and surface coils at 64 and 300 MHz," *J. Magn. Reson. Imaging*, vol. 19, no. 5, pp. 650–656, 2004.
- [54] X. Zhang, J. Liu, S. Schmitter, P.-F. van de Moortele, and B. He, "Predicting temperature increase through local SAR estimation by B_1 mapping: A phantom validation at 7T," in *Proc. 36th Annu. Int. Conf. Engineering Medicine Biology Society*, 2014, pp. 1107–1110.
- [55] Z. Wang, J. C. Lin, W. Mao, W. Liu, M. B. Smith, and C. M. Collins, "SAR and temperature: Simulations and comparison to regulatory limits for MRI," *J. Magn. Reson. Imaging*, vol. 26, no. 2, pp. 437–441, 2007.
- [56] N. Boulant, U. Katscher, M. Luong, A. Massire, A. Amadon, and A. Vignaud, " B_1^+ -based SAR assessment using a birdcage coil at 7 Tesla: Experimental evaluation using magnetic resonance thermometry," in *Proc. Int. Society Magnetic Resonance Medicine*, 2014, vol. 22, p. 4900.
- [57] Y. Nikawa, "Application of microwaves in medical sensing and treatment," in *Proc. Asia-Pacific Microwave Conf.*, 2013, pp. 62–64.
- [58] R. W. Cox, "fMRI analysis methods: Classics and new trends," in *Proc. Int. Society Magnetic Resonance Medicine*, 2014, vol. 22, pp. 1–4.
- [59] M. Kaiser, J. Krug, and G. Rose, "Interventional MRI: Minimal invasive surgery under MR guidance," in *IEEE MTT-S Int. Microwave Symp. Dig.*, 2011, pp. 1–4.
- [60] P. R. Luijten, "The physicist's view of UHF of humans," in *Proc. Int. Society Magnetic Resonance Medicine*, 2014, vol. 22, p. 0233.
- [61] C. Z. Cooley, J. P. Stockmann, B. D. Armstrong, M. Sarracanie, M. H. Lev, M. S. Rosen, and L. L. Wald, "2D imaging in a lightweight portable MRI scanner without gradient coils," in *Proc. Int. Society Magnetic Resonance Medicine*, 2014, vol. 22, p. 21.
- [62] S. F. Ahmad, Y. C. Kim, H. W. Son, Y. K. Cho, and H. D. Kim, "RF receiver coil with dual resonance frequencies for small animal MRI system," in *Proc. IEEE Middle East Conf. Antennas Propagation*, Oct. 20–22, 2010, pp. 1–5.

